Biogeosciences Discuss., 10, 6939–6972, 2013
www.biogeosciences-discuss.net/10/6939/2013/
doi:10.5194/bgd-10-6939-2013

Biogeosciences Discussions
Open Access

Impact of the Kuroshio intrusion on the nutrient inventory in the upper northern South China Sea: insights from an isopycnal mixing model

C. Du[1], Z. Liu[1], M. Dai[1], S.-J. Kao[1], Z. Cao[1], Y. Zhang[2], T. Huang[1], L. Wang[1], and Y. Li[1]

[1]State Key Laboratory of Marine Environmental Science, Xiamen University, Xiamen 361005, China
[2]Key Laboratory of Coastal Zone Environmental Processes, Yantai Institute of Coastal Zone Research, Chinese Academy of Sciences, Yantai 264003, China

Received: 29 March 2013 – Accepted: 5 April 2013 – Published: 18 April 2013

Correspondence to: M. Dai (mdai@xmu.edu.cn)

Published by Copernicus Publications on behalf of the European Geosciences Union.

Abstract

Based on four cruises covering a seasonal cycle in 2009–2011, we examined the impact of the Kuroshio intrusion, featured by extremely oligotrophic waters, on the nutrient inventory in the central northern South China Sea (NSCS). The nutrient inventory in the upper 100 m of the water column in the study area ranged from ~200 to ~290 mmol m^{-2} for N + N (nitrate plus nitrite), from ~13 to ~24 mmol m^{-2} for soluble reactive phosphate and from ~210 to ~430 mmol m^{-2} for silicic acid. The nutrient inventory showed a clear seasonal pattern with the highest value appearing in summer, while the N + N inventory in spring and winter had a reduction of ~13 % and ~30 %, respectively, relative to that in summer. To quantify the extent of the Kuroshio intrusion, an isopycnal mixing model was adopted to derive the proportional contribution of water masses from the SCS proper and the Kuroshio along individual isopycnal surfaces. The derived mixing ratio along the isopycnal plane was then employed to predict the genuine gradients of nutrients under the assumption of no biogeochemical alteration. These predicted nutrient concentrations, denoted as N_m, are solely determined by water mass mixing. Results showed that the nutrient inventory in the upper 100 m of the NSCS was overall negatively correlated to the Kuroshio water fraction, suggesting that the Kuroshio intrusion significantly influenced the nutrient distribution in the SCS and its seasonal variation. The difference between the observed nutrient concentrations and their corresponding N_m allowed us to further quantify the nutrient removal/addition associated with the biogeochemical processes on top of the water mass mixing. We revealed that the nutrients in the upper 100 m of the water column had a net consumption in both winter and spring but a net addition in fall.

BGD
10, 6939–6972, 2013

1 Introduction

The major ocean basins at low latitudes are often nutrient depleted in their upper mixed layer because strong stratification in the pycnocline diminishes nutrient supplies from the depths through diapycnal mixing (Lewis et al., 1986). While coastal oceans are typically characterized by higher nutrient concentrations due to abundant riverine inputs at the surface (e.g. Cai et al., 2004; Chen and Chen, 2006; Han et al., 2012) and elevated supplies from the depths through processes such as strong upwelling and/or enhanced diapycnal mixing (e.g. Bourgault et al., 2011; Gong et al., 1992; Tian et al., 2009), the deep basins of some large marginal seas in low latitudes are overall oligotrophic due partly to the year-round stratification (e.g. Thingstad et al., 2005; Wu et al., 2003). On the other hand, some marginal seas are strongly influenced by the boundary currents of the adjacent open ocean (Chen, 2008; Gordon, 1967; Huertas et al., 2012; Matsuno et al., 2009; Qu et al., 2000) which are usually very oligotrophic. An example is the Kuroshio of the North Pacific Ocean, which is featured by extremely low nutrients. Nutrients within the marginal seas may thus be significantly impacted by permanent or occasional intrusions of the boundary currents. Although the interactions between the open oceans and the marginal seas have been extensively studied in terms of their water exchanges and the dynamic controls (e.g. Baringer et al., 1999; Chu and Li, 2000; Hu et al., 2000; Kida et al., 2009; Liang et al., 2008; Matsuno et al., 2009; Partt and Spall, 2008; Qu et al., 2000; Shaw, 1991; Tian et al., 2006), their impacts on the nutrient inventory of the marginal seas and the consequent biogeochemical effects have rarely been examined (Huertas et al., 2012).

The South China Sea (SCS), which is the largest marginal sea of the Pacific, is under significant modulation by water exchanges through the Luzon Strait. It is well known that the Kuroshio carries the most oligotrophic water of the world's oceans and that it intrudes into the SCS at least in winter (e.g. Centurioni et al., 2004; Chen et al., 2001; Chu and Li, 2000; Hu et al., 2000; Qu, 1999; Qu et al., 2000). However, the

BGD
10, 6939–6972, 2013

impact of the Kuroshio intrusion on the upper ocean nutrient inventory in the SCS has rarely been assessed in a quantitative way.

In this study, a large data set of nutrients including N / P/Si was collected during four cruises to the northern SCS (NSCS) covering a complete seasonal cycle. The nutrient inventory of the upper 100 m in each season was calculated and compared. Moreover, an isopycnal mixing model was developed to quantitatively estimate the seasonal intrusion pattern of the Kuroshio to the NSCS. Based on a combination of field observations and the model calculation, the Kuroshio's influence on the upper 100 m nutrient inventory of the NSCS was further quantified and the biogeochemical processes on top of the isopycnal mixing scheme were examined.

2 Materials and methods

2.1 Study area

The seasonally reversing East Asian Monsoon drives clockwise circulation in summer and anticlockwise circulation during winter in the upper SCS. As a consequence, the interior of the SCS is effectively isolated from terrestrial inputs and forms a basin-wide gyre, which displays overall oligotrophic characteristics similar to those in the major ocean basins (Gong et al., 1992). On the other hand, the SCS and the western North Pacific (wNP) exchange their water masses via the 2200 m deep Luzon Strait, through which the Kuroshio Branch Water intrudes from the wNP into the SCS (Chen, 2001; Chu and Li, 2000; Dai et al., 2009; Hu et al., 2000; Qu et al., 2000) (Fig. 1). It is reported that at the salinity maximum layer, at a depth of ∼ 150 m, the Kuroshio intrudes into the SCS all year round (Qu et al., 2000).

2.2 Sampling and analyses

Field observations were carried out in summer (July–August, 2009), winter (January, 2009), fall (October–November, 2010) and spring (April, 2011). The sampling area

BGD
10, 6939–6972, 2013

covered nearly the entire NSCS except in the fall cruise when only the western part of the NSCS was covered due to high sea conditions. In this study, we focused on the central NSCS covering a region from 111 to 119.5° E and from 17.7° N to roughly the 200 m isobaths in the meridional direction (Fig. 1). The total surface area of the subject zone is about 2.74×10^{11} m^2. We excluded the shelf shallower than 200 m (Fig. 1) where the nutrient inventories are under significant influence by the riverine inputs.

Nutrient samples were collected with a Rosette sampler and analyzed onboard using a Four-channel Continuous Flow Technicon AA3 Auto-Analyzer (Bran-Lube GmbH). The detection limits for N + N (nitrate plus nitrite), SRP (soluble reactive phosphate) and $Si(OH)_4$ (silicic acid) were 0.03 µmol L^{-1}, 0.03 µmol L^{-1} and 0.05 µmol L^{-1}, respectively. The analytical precision was better than ±1 % for N + N, ±2 % for SRP and ±2.8 % for $Si(OH)_4$ (Han et al., 2012). In addition, SRP was determined at nanomolar levels in the surface waters. The SRP in the water samples was pre-concentrated as phosphomolybdenum blue into a solid phase cartridge (Waters Oasis), then eluted with sodium hydroxide solution, and finally determined using a spectrophotometer within a flow injection system. The detection limit of this method is 1.4 nmol L^{-1} and the precision is better than ±5 % (Ma et al., 2008; Han et al., 2012). Depth profiles of temperature and salinity were determined shipboard with the SBE911 Conductivity-Temperature-Depth (CTD) recorder (Sea-Bird Co.).

2.3 Estimation of the nutrient inventory

Using field measured nutrient concentrations, we estimated both the station-integrated and area-integrated nutrient inventories in the central NSCS. The former was calculated by integrating nutrient concentrations in the upper 100 m of the water column at individual stations. The latter was obtained by integrating the station-integrated nutrient inventories over the entire study area via spatial interpolations, for which the Inverse Distance Square method was applied (Lin et al., 2002).

BGD
10, 6939–6972, 2013

3 Results

3.1 Hydrography

As shown in Fig. 2, the Potential Temperature–Salinity (θ–S) distributions in the upper 400 m of the water column revealed a distinct hydrological difference between the central NSCS and the Kuroshio, with the latter being indicated by data points collected along sections LU5 and LU6. At density levels of $< 1025.7\,kg\,m^{-3}$, which corresponded to the depth of < 200 m in the NSCS and < 350 m in the Kuroshio, the Kuroshio water tended to have higher potential temperature and salinity than the SCS water. However, the pattern was reversed at greater depths (Fig. 2). Among the four seasons, the summer θ–S distribution pattern in the central NSCS was least close to that of the Kuroshio water, and the data points in the upper 200 m in summer were overall less scattered relative to those during spring, fall and winter, due likely to the higher extent of the Kuroshio intrusion in the latter three seasons. At density levels of $> 1026.2\,kg\,m^{-3}$ (corresponding to the depth of > 300 m in the NSCS), no significant seasonal variations of θ–S distributions were observed in the central NSCS.

Since biological alterations of nutrients are highest in the euphotic zone, which typically extends from the surface to ~ 100 m water depth in the SCS (Chen et al., 2008; Tseng et al., 2005), we focused on the nutrient dynamics in the upper 100 m of the central NSCS.

3.2 Nutrient distribution in the upper 100 m of the central NSCS and the Kuroshio

Since the distribution patterns of N + N, SRP and $Si(OH)_4$ were similar, we used N + N as an example throughout this paper unless otherwise indicated. The spatial and temporal distributions of the iso-depth N + N concentration are shown in Fig. 3. During spring and summer, the surface N + N concentration in the entire central NSCS was mostly below the detection limit of quantification, or $< 0.1\,\mu mol\,L^{-1}$ (Fig. 3a, b). Similarly

BGD
10, 6939–6972, 2013

in fall, the surface N + N concentrations at the majority of the sampling stations were below the detection limit, except at the four stations located in the central basin which displayed a relatively high N + N concentration of ~ 1.5 μmol L^{-1} (Fig. 3c). This region was characterized by low sea surface temperature (data not shown), possibly indicating that the strong wind-driven mixing process in fall drew nutrient-rich waters from the depths. In winter, the surface N + N concentration ranged between 0–1.2 μmol L^{-1}, which was slightly higher than that in other seasons (Fig. 3d).

Nutrient concentrations increased rapidly with depth as shown in Fig. 3e–l. During spring, high nutrient centers with N + N > 2 μmol L^{-1} and > 10 μmol L^{-1} were observed at 50 m (Fig. 3e) and 100 m (Fig. 3i), respectively, in the central part of the NSCS. In this region, low temperature and high salinity were observed at 75 m and 100 m, and sea surface height analysis also showed low values in the same region, which indicated that a cyclonic circulation occurred in this region, and might have induced this high N + N center. In summer, N + N distributions showed significant spatial variations in the central NSCS, with higher concentrations in the western part (> 1 μmol L^{-1} at 50 m and > 10 μmol L^{-1} at 100 m) and lower ones in the eastern part (< 1 μmol L^{-1} at 50 m and < 10 μmol L^{-1} at 100 m) (Fig. 3f, j). During fall, N + N concentrations at 50 m were relatively higher in the middle and southern regions (> 2 μmol L^{-1}) than those in the western and eastern regions (< 1 μmol L^{-1}) of the NSCS (Fig. 3g). At 100 m however, higher values were observed in the western part (~ 10 μmol L^{-1}) while lower values were observed in the eastern part (~ 5 μmol L^{-1}) (Fig. 3k). In winter, a broad zone with low nutrient levels was located along the shelf break, corresponding to an N + N concentration of 0–2 μmol L^{-1} at 50 m (Fig. 3h) and 2–10 μmol L^{-1} at 100 m (Fig. 3l). Meanwhile, a high N + N concentration zone was observed along section E4 in the northeast part of the central NSCS (Fig. 3h, l).

BGD
10, 6939–6972, 2013

3.3 Comparison of nutrient distributions between the central NSCS and the Kuroshio waters

Vertical distributions of potential temperature and SRP in the upper 200 m at the SEATS (South East Asian Time-series Study, Wong et al., 2007) and LU65 stations, which were representative of the SCS and Kuroshio waters, are shown in Fig. 4. Significant seasonal patterns were observed at the SEATS station. Its upper mixed layer depth (optimal estimation of $\Delta T = 0.8\,^{\circ}\mathrm{C}$ according to Kara et al., 2000) is deeper in winter (~ 60 m) than in spring (~ 10 m), summer (~ 35 m) and fall (~ 40 m) (Fig. 4a). On the other hand, SRP concentrations in the mixed layer were higher in fall ($\sim 0.08\,\mu\mathrm{mol\,L^{-1}}$) than those in spring ($\sim 0.04\,\mu\mathrm{mol\,L^{-1}}$), summer ($\sim 0.02\,\mu\mathrm{mol\,L^{-1}}$) and winter ($\sim 0.03\,\mu\mathrm{mol\,L^{-1}}$) (Fig. 4b). At the same depth above 200 m, the Kuroshio water was relatively warmer by 0–8 °C and the SRP lower by 0–1.1 $\mu\mathrm{mol\,L^{-1}}$ than the SCS water. In this context, intrusions of the Kuroshio water with low nutrient content might have induced a dilution effect on the NSCS nutrients.

3.4 Nutrient inventory in the upper 100 m of the central NSCS

The station-integrated N + N inventory in the upper 100 m of the central NSCS is shown in Fig. 5. The N + N inventory ranged from 50–600 $\mathrm{mmol\,m^{-2}}$ in spring (Fig. 5a). A high N + N inventory center of $> 500\,\mathrm{mmol\,m^{-2}}$ was observed in the central basin of the NSCS, which was about twice that at the edge stations (~ 100–$200\,\mathrm{mmol\,m^{-2}}$). Regions with the N + N inventory $< 100\,\mathrm{mmol\,m^{-2}}$ were observed at the northeast part near Taiwan and the southwest part near Hainan. During summer (Fig. 5b), the station-integrated N + N inventory was mostly $> 300\,\mathrm{mmol\,m^{-2}}$ in the entire central NSCS, whereas the $< 100\,\mathrm{mmol\,m^{-2}}$ region was observed only at the western part. In fall, the N + N inventory was higher in the western part ($> 300\,\mathrm{mmol\,m^{-2}}$), but lower in the eastern part ($< 100\,\mathrm{mmol\,m^{-2}}$) (Fig. 5c). During winter, a band with low N + N inventory ($< 200\,\mathrm{mmol\,m^{-2}}$) was located between the Luzon Strait and 115° E along the shelf break in the northeast part of the central NSCS (Fig. 5d), in which an extremely low

BGD
10, 6939–6972, 2013

N + N inventory center ($\sim 20\,\mathrm{mmol\,m^{-2}}$) was observed. Combined with the iso-depth distributions (Fig. 3), the N + N inventory information revealed an overall pattern that the nutrients were consistently higher in the western than in the eastern part of the central NSCS.

On the basis of these seasonal observations, the annual averaged N + N inventory was estimated to be $\sim 250\,\mathrm{mmol\,m^{-2}}$ in the central NSCS, which was significantly higher than that in the Kuroshio in spring, implying again the potential dilution effect of the Kuroshio intrusion on the nutrient inventory of the upper NSCS.

Taking the central NSCS as a whole, the area-integrated N + N inventory (see Sect. 2.3 for details) was highest in summer, while it was ~ 13, ~ 16 and ~ 32 % lower in spring, fall and winter, respectively, as compared to that in summer (Table 1). The seasonal patterns of the SRP and $Si(OH)_4$ inventories were similar to that of N + N but with larger degrees of reduction in winter as compared to N + N (Table 1).

4 Discussion

4.1 Water fraction estimation with the isopycnal mixing approximation

In exploring the seasonal intrusions of the Kuroshio to the central NSCS, we assumed that the mixing between different water masses was mainly along isopycnal surfaces, while the diapycnal processes which occurred were insignificant. This statement can be approached by means of a comparison between the diffusive flux along and across isopycnal surfaces.

According to Fick's law of diffusion, the diffusive flux of dissolved material can be expressed as:

$$F = -K \times \partial c/\partial x. \quad (1)$$

where K can be either the diapycnal (K_V) or isopycnal (K_H) diffusivity, and $\partial c/\partial x$ is the corresponding concentration gradient. At an isopycnal surface at about 100 m in

BGD
10, 6939–6972, 2013

the central NSCS, we adopted the K_V of $10^{-5}\,m^2\,s^{-1}$ according to Liu and Lozovatsky (2012) and the K_H of $500\,m^2\,s^{-1}$ based on Glover et al. (2005). The horizontal gradient in N + N was $\sim 1.0 \times 10^{-5}\,mmol\,m^{-4}$ based on the estimated distance of 750 km and a concentration difference of about 10 mmol m^{-3} in N + N between section LU6 of the Kuroshio and the central NSCS. At the same time, the vertical gradient in N + N at the SEATS station was estimated to be $\sim 1 \times 10^{-1}\,mmol\,m^{-4}$ at the 100 m layer. Based on Eq. (1), the isopycnal flux was estimated to be $5.0 \times 10^{-3}\,mmol\,m^{-2}\,s^{-1}$, which was three orders of magnitude larger than the diapycnal flux of $1.0 \times 10^{-6}\,mmol\,m^{-2}\,s^{-1}$. This suggested that isopycnal mixing was indeed prevailing over diapycnal diffusion in controlling the physical transport of nutrients in the upper central NSCS. Note that the K_H adopted from Glover at al. (2005) should be regarded as a lower limit and thus the actual difference between the isopycnal and diapycnal fluxes might be even larger.

The mixing ratio of the Kuroshio water and the SCS proper water along any isopycnal surface can be quantitatively determined, the detailed methodology of which can be illustrated with reference to the θ–S diagram (Fig. 6). Firstly, following previous studies (e.g. Chen and Huang, 1996; Gong et al., 1992), the two end-members representing typical Kuroshio water and SCS proper water were chosen as the precursors of the NSCS water under consideration. For any in situ observed water parcel represented by a point in the θ–S diagram, the fractional contributions of Kuroshio and SCS water can be derived by adopting the conservative along-isopycnal mixing law of θ or S:

$$R_K = R_{k\_\theta} = \frac{\theta - \theta_S}{\theta_K - \theta_S}$$
$$R_K = R_{k\_S} = \frac{S - S_S}{S_K - S_S} \quad (2)$$

Here, the Kuroshio water fraction is denoted as R_K (R_{K_θ} and R_{K_S} represent results derived from θ and S, respectively), and thus $1 - R_K$ stands for the SCS proper water fraction. θ_K and S_K denote the end-member values of θ and S for the Kuroshio water, while θ_S and S_S represent those for the SCS proper water. Due to the fact that the

BGD
10, 6939–6972, 2013

thermal structures in the upper ocean are significantly influenced by the seasonally varying heat flux (Tseng et al., 2005), we used S conservation for the upper 60 m of the water column for model prediction. At greater depths, θ was used due to its higher sensitivity than salinity (Fig. 6a). The model derived R_K at each sampling point in the upper 400 m of the central NSCS is shown in Fig. 6a.

As an example, R_K for a water parcel located at the potential density anomaly surface of 23.5 is also shown in Fig. 6a. According to the isopycnal mixing approximation, this water parcel was a mixture of the SCS end-member and the Kuroshio end-member with the same potential density of 23.5 (as the nonlinear mixing of the density, the genuine potential density anomaly of its parents are slightly higher than 23.5). As such, R_K was estimated to be 0.4, meaning that the fractional contribution from the Kuroshio was 40 %, while the SCS endmember contributed 60 % to the mixture.

As shown in Fig. 6b, there was an along-isopycnal surface difference of $\sim$0–10 µmol L^{-1} in N + N in the upper 100 m of the water column between the typical SCS and the Kuroshio. With the derived water fractions, the nutrient concentrations (N_m) of each water parcel in the central NSCS could be calculated from

$$N_m = R_K \times N_K + (1 - R_K) \times N_S \quad (3)$$

This is the nutrient concentration solely due to conservative physical mixing of the parent waters. In situ observed concentrations might have departed from this value due to chemical and/or biological alterations. Here, N_K and N_S are the end-member concentrations of nutrients for the Kuroshio and the SCS proper water at a given isopycnal surface.

4.2 Model validation and error estimation

Since the seawater-dissolved calcium ion (Ca^{2+}) is nearly conservative in the upper ocean, despite possible small changes resulting from $CaCO_3$ production or dissolution (Cao and Dai, 2011; Feely et al., 2002), we could use the high-precision data of Ca^{2+} to evaluate the applicability of our isopycnal mixing approach.

BGD
10, 6939–6972, 2013

As shown in Fig. 7a, the isopycnal mixing approximation worked very well in predicting concentrations of Ca^{2+} in the upper 100 m of the central NSCS; the model-prediction and the observations were highly correlated ($R = 0.993$, $n = 96$, $p < 0.0001$), and the slope was 0.93, suggesting a 7 % bulk uncertainty of the model prediction. This provided direct evidence for the applicability of our isopycnal mixing model.

However, observable departures in model prediction from field measurements did exist, which provided an estimate of the errors in the estimated water fractions induced by the physical approximations adopted in the isopycnal mixing model.

If r is the error in the derived Kuroshio water fraction (R_K) and assuming Ca^{2+} to be perfectly conservative (i.e. the observed Ca^{2+} is solely a result of water mass mixing without any chemical or biological alterations), we have

$$\begin{aligned} Ca_M^{2+} &= R_K \times Ca_K^{2+} + (1-R_K) \times Ca_S^{2+} \\ Ca_F^{2+} &= (R_K + r) \times Ca_K^{2+} + (1-R_K-r) \times Ca_S^{2+} \end{aligned} \quad (4)$$

Here, Ca_M^{2+} and Ca_F^{2+} denote the model derived and field observed Ca^{2+} concentrations, respectively, and Ca_K^{2+} and Ca_S^{2+} are the end-member concentrations of Ca^{2+} for Kuroshio and SCS proper water, respectively. Therefore, the error in each individual estimate of R_K is

$$r = \frac{Ca_M^{2+} - Ca_F^{2+}}{Ca_K^{2+} - Ca_S^{2+}} \quad (5)$$

As shown in Fig. 7b, the absolute value of r in the upper 100 m of the central NSCS was mostly < 0.1, or less than 10 %. Statistically, it had a mean value of -0.02 (X_r), and a standard deviation of 0.09 (S_r, $n = 96$). Note that this error r derived from Ca^{2+} is an upper limit estimate of the model error, as it also includes errors due to potential $CaCO_3$ production or dissolution.

BGD
10, 6939–6972, 2013

Besides model approximations, the selection of end-members also introduced uncertainties to the results. This is detailed in the Supplement. Overall, the uncertainty resulting from the SCS end-member variation was $-0.09 \pm 0.28\,\mu mol\,L^{-1}$ (the mean value (X_{NS}) ± standard deviation (S_{NS}) is the same in the following descriptions) for N + N, $0.026 \pm 0.015\,\mu mol\,L^{-1}$ for SRP and $0.48 \pm 0.30\,\mu mol\,L^{-1}$ for $Si(OH)_4$. On the other hand, the uncertainty induced by the Kuroshio end-member variation was $-0.22 \pm 0.38\,\mu mol\,L^{-1}$ for N + N, $-0.002 \pm 0.030\,\mu mol\,L^{-1}$ for SRP and $-0.28 \pm 0.59\,\mu mol\,L^{-1}$ for $Si(OH)_4$.

Combining the model induced error r and the uncertainties introduced by the selection of end-members, the total error for the estimated nutrient concentration (Eq. 3, see Supplement for details) was averaged to be about $-0.16 \pm 0.65\,\mu mol\,L^{-1}$ for N + N ($X_N \pm S_N$), $-0.002 \pm 0.043\,\mu mol\,L^{-1}$ for SRP and $0.1 \pm 0.73\,\mu mol\,L^{-1}$ for $Si(OH)_4$ in the upper 100 m of the central NSCS. The negative values indicate overestimation of the model.

4.3 Impact of the Kuroshio intrusion on the nutrient inventory in the central NSCS

The Kuroshio water fraction (R_K; Eq. 2) for each water parcel was integrated over the upper 100 m for a given station to represent the station-integrated Kuroshio water fraction (R_{IKW}). Similarly, we calculated the station-integrated Kuroshio nutrient fraction (R_{IKN}) according to the following equation:

$$R_{IKN} = \frac{I_{KN}}{I_N} = \frac{\sum_{z=0}^{z=100\,m} R_K \times N_K}{\sum_{z=0}^{z=100\,m} (N_m)} \quad (6)$$

where I_N is the station-integrated nutrient concentration in the upper 100 m of the central NSCS, and I_{KN} is the nutrient contribution from the Kuroshio water.

BGD
10, 6939–6972, 2013

As shown in Fig. 8a–d, the spatial distribution of R_{IKW} displayed distinct features over the seasons. In spring, fall and winter, the R_{IKW} was typically above 0.2 in the northeast part of the central NSCS under the stronger influence of the Kuroshio intrusion (Fig. 8a, c and d). In summer, R_{IKW} was < 0.2 except in the region near the Luzon Strait (Fig. 8b). Relative to that in summer, R_{IKW} in fall was slightly higher in the eastern part (> 0.2) while lower in the west (< 0.1) (Fig. 8c). Nevertheless, it was clear from the spatial distributions in different seasons that the Kuroshio influence in the central NSCS was persistent all year round, although varying in magnitude. Evidently, the intrusions reached maximum in the north part of the study area in spring and in winter under study.

The patterns of the R_{IKN} distribution resembled that of R_{IKW}, but the value of the former was much lower. Most notably, only a very small fraction of the Kuroshio water was observed during summer in the central NSCS (Fig. 8b), again suggesting that the Kuroshio did not significantly intrude into the SCS in summer. The basin wide surface circulation of the SCS in summer responding to the Southwest monsoon may prevent the Kuroshio from further intrusion (if any) into the interior of the SCS and, instead, it flows out eastwardly through the Luzon Strait (Chu and Li., 2000; Hu et al., 2000; Qu et al., 2000). The lowest R_{IKW} was ~ 0.06 in summer and the highest R_{IKW} was ~ 0.3 in spring, a difference which suggested that about 24 % of the water exchanged with the Kuroshio in one seasonal cycle. Accordingly, the resident time of waters in the upper 100 m of the central NSCS could be estimated to be 4.1 yr, which is comparable to the 4.7 yr for waters in the upper 350 m of the SCS estimated by Chen et al. (2001).

As shown in Fig. 9a, the model predicted N + N (N_m) agreed well overall with the field measurements. The fact that the majority of the scattered data points fell outside the estimated N + N error ($X_N \pm S_N$) domain may suggest significant biological mediation of the nutrient, in particular in the upper layer of the central NSCS (Fig. 9a). As shown in Fig. 9b, the field estimated N + N inventory was overall negatively correlated with the corresponding R_{IKW}. The even distribution of the data points around the theoretical

BGD
10, 6939–6972, 2013

mixing line indicated that the Kuroshio intrusion might play a key role in the N + N inventory of the study area.

In order to assess the dilution effect of the Kuroshio intrusion, featured by extremely low nutrients, we calculated the area-integrated Kuroshio dilution amount (K_{NR}) of the nutrient inventory over the upper 100 m of the central NSCS based on the proposed isopycnal mixing model as:

$$K_{NR} = \sum^{area} \left(\sum_{z=0\,m}^{z=100\,m} (N_S) - \sum_{z=0\,m}^{z=100\,m} (N_m) \right) \quad (7)$$

Here, N_S is the SCS endmember nutrient concentration before Kuroshio dilution, and N_m is the model predicted nutrient. Assuming that the study area is under steady state on an intra-seasonal time scale, we did a first order estimate of the nutrient inventory reduction from summer 2009 to winter 2009. The calculated K_{NR} values were $\sim 21 \times 10^9$, $\sim 1.5 \times 10^9$ and $\sim 22 \times 10^9$ mol for N + N, SRP and $Si(OH)_4$, respectively. The nutrient inventory reduction values in winter 2009 relative to those in summer 2009 were $\sim 25 \times 10^9$, $\sim 3 \times 10^9$ and $\sim 60 \times 10^9$ mol for N + N, SRP and $Si(OH)_4$, respectively (Table 1). As a consequence, the Kuroshio intrusion accounted for an inventory reduction of ~ 83, ~ 52 and ~ 37 % for N + N, SRP and $Si(OH)_4$ during this period of time, whereas the residual reduction might be attributed to the biological metabolism and/or other physical processes. It should be pointed out that these reduction assessments are referenced to summer 2009, while our four surveys spanned from 2009 to 2011. Therefore, our estimated reduction at seasonal levels assumed no interannual variations in the Kuroshio intrusions into the SCS, which is however not always true (e.g. Chao et al., 1996; Michael et al., 2006; Liu et al., 2011).

It might be argued that other processes also regulate the N + N inventory in the upper ocean. One additional possible process to supply nutrients is N_2-fixation. However, N_2-fixation is estimated to be $\sim 20\,mmol\,N\,m^{-2}\,yr^{-1}$ in the NSCS (Kao et al., 2012), which only accounts for less than 10 % of the present nutrient inventory variation ($\sim 250\,mmol\,m^{-2}$). Moreover, N_2-fixation is a net sink for the N + N inventory which

BGD
10, 6939–6972, 2013

accounts for the increase in the N + N inventory, while the reduction in the nutrient inventory we observed occurred in the second half of 2009. Thus, the genuine inventory reduction might exceed our estimation. Another possible process to add nutrients is diapycnal mixing. In particular, during the strong northeast monsoon season, deepening of the surface mixed layer frequently occurs, which enhances the influxes of the nutrient-rich subsurface water (Tseng et al., 2005; Liu et al., 2002). As a result, an enhancement by ~2 fold in primary production in the central NSCS is reported in winter as compared to that in summer (Chen, 2005; Chen and Chen, 2006). However, based on turbulence profiling measurements (data not shown), we estimated the upward N + N flux across the 100 m layer to be ~0.1 mmol m^{-2} d^{-1}, implying that it might take more than ~7 yr to thoroughly change the N + N inventory given the averaged N + N inventory of ~250 mmol m^{-2} in the upper 100 m of the central NSCS. Therefore, we contend that on a seasonal time scale, the effect of diapycnal mixing on the N + N inventory might be negligible.

The Kuroshio intrusion might also affect the nutrient ratio stoichiometry in the central NSCS, due to the observably different Si/N and N / P ratios between the SCS proper and the Kuroshio water at the same isopycnal surface. Potentially attributable to N_2-fixation (e.g. Kao et al., 2012) and upwelling (Gong et al., 1992), the N / P ratio of the upper 100 m ranged from 0.2–14.5 in the SCS, which is generally higher than that in the Kuroshio of 0.1–10 in the upper 150 m. The intrusion of the Kuroshio and its seasonal contrast might therefore significantly shape the nutrient ratio structure in the SCS, which would have a fundamental impact on the ecosystem structure therein.

4.4 Biogeochemical alteration of nutrients in the upper 100 m of the central NSCS

Although the model predicted N + N concentrations and the field measurements showed an overall agreement in the upper 100 m of the central NSCS, observable departures did exist (Fig. 9a and 10). The difference, denoted here as Δ, would suggest a biogeochemically mediated portion of the nutrients. As shown in Fig. 10a, the majority

BGD
10, 6939–6972, 2013

of the departures occurred in the upper euphotic zone where N + N concentrations were lower than 10 µmol L^{-1}.

For Δ(N + N) and ΔSRP, a scatter distribution ranging from −6 to 6 µmol L^{-1} and −0.3 to 0.4 µmol L^{-1} were found in the upper 100 m of the central NSCS (Fig. 10a, b). The histogram distributions further showed that the majority of these data could be grouped between ±2 µmol L^{-1} for Δ(N + N) and ±0.15 µmol L^{-1} for ΔSRP (90 % data range; Fig. 10d, e). As shown by the seasonal moving average line, both Δ(N + N) and ΔSRP values were positive in spring and winter but negative in fall (Fig. 10a, b). We inferred that on average ∼ 0–3 µmol L^{-1} of N + N and ∼ 0–0.15 µmol L^{-1} of SRP were removed by biological metabolism in the upper 100 m of central NSCS during winter and spring. Such removal was much more significant in the upper 50 m in winter, which agreed well with the fact that the primary production is generally higher in winter in the NSCS (Chen, 2005; Chen and Chen, 2006). In summer, both Δ(N + N) and ΔSRP were around zero, suggesting no significant biological consumption of nutrients. In contrast, in fall, Δ(N + N) and ΔSRP were overall negative suggesting net nutrient addition in the upper central NSCS.

If we further assumed that our study area was under steady state on a seasonal time scale, the above removal of nutrients would be translated into a new production of about 6.0 ± 2.7 mmol C m^{-2} d^{-1} in spring, 1.8 ± 2.7 mmol C m^{-2} d^{-1} in summer, −4.5 ± 2.7 mmol C m^{-2} d^{-1} in fall and 7.4 ± 2.7 mmol C m^{-2} d^{-1} in winter based on the C/N Redfield ratio of 106/16 (Redfield et al., 1963). The negative value in fall might indicate that nutrient addition was larger than its removal inducing no net production.

It should be pointed out that the above derived new production values in spring and summer were very close to those previously reported in the NSCS basin (∼ 5.8 mmol C m^{-2} d^{-1} in spring, ∼ 2.5 mmol C m^{-2} d^{-1} in summer), based on the ^{15}N incubation method (Chen, 2005). However, our derived value in winter was substantially lower than the reported value of ∼ 21.7 mmol C m^{-2} d^{-1} (Chen, 2005), and our derived data in fall was significantly different from the reported value of ∼ 4.1 mmol C m^{-2} d^{-1}. The reasons for the discrepancy in the fall and winter new production estimates are

BGD
10, 6939–6972, 2013

unclear and require additional studies. We also note that the field measurements in winter have been extremely sparse in the SCS as elsewhere in the world ocean.

Nevertheless, our derived $\Delta(N+N)/\Delta SRP$ ratio, or the relative biological consumption, with its average value of ~12.8 was in very good agreement with the Redfield Ratio (Redfield et al., 1963) (Fig. 10c, f). This ratio was also consistent with the (N + N)/SRP ratio obtained from the depths in the SCS, the average of which is around 13.6 based on long term observations at SEATS (Wong et al., 2007). Such consistence provided another piece of evidence that our isopycnal mixing model was generally in order. Among different seasons, the $\Delta(N+N)/\Delta SRP$ ratio diagnosed from the model, which is the slope of the linear regression line between $\Delta(N+N)$ and ΔSRP, was highest in fall (~17.8, $R = 0.97$, $n = 66$, $P < 0.0001$), but lowest in winter (~9.2, $R = 0.79$, $n = 88$, $P < 0.0001$). This ratio was ~13.4 in spring ($R = 0.93$, $n = 168$, $P < 0.0001$) and ~12.4 in summer ($R = 0.88$, $n = 135$, $P < 0.0001$), both of which were close to the average value of ~12.8. Quigg et al. (2003) report a different phytoplankton composition associated with different element composition, and so a different $\Delta(N+N)/\Delta SRP$ addition/removal ratio in the NSCS might indicate that a red superfamily (lower N / P ratio demand) was prevailing in winter, and a green superfamily (high N / P ratio demand) in fall.

5 Conclusions

Both nutrient concentrations and their inventory in the upper 100 m of the central NSCS displayed significant spatial and seasonal variations. The inventories were overall higher in the west part relative to the east part of the central NSCS, which is consistent with the decreasing dilution effect along the travel path of the Kuroshio intrusion. On a seasonal time scale, the nutrient inventories in the upper 100 m were relatively high in summer but low in spring and winter. In addition to the mesoscale eddy and regional upwelling, the Kuroshio intrusion might therefore play a dominant role in determining the nutrient inventory distribution in the central NSCS.

BGD
10, 6939–6972, 2013

A two end-member based isopycnal mixing model was adopted to derive the Kuroshio and SCS proper water fractions in the water parcel of the central NSCS, and this indicated that spring and winter were the two main seasons for the Kuroshio water fraction distribution in the central NSCS. The station-integrated Kuroshio water fraction showed a significant negative correlation with the nutrient inventory in the upper 100 m of the central NSCS, indicating the dominant Kuroshio dilution effect. Based on the end-member sensitivity analysis and water fraction error estimation, our well-validated model results demonstrated relatively high nutrient consumption during winter and spring but possibly net addition in fall in the upper 100 m of the central NSCS.

It is important to note that the SCS does not have its own independent water mass formation since, on a time scale > 4 yr longer than the resident time of the SCS surface water (Chen, 2001), the SCS water originally came from the wNP, although with a certain degree of transformation. We thus caution applying the isopycnal mixing approach to quantify the impact of the Kuroshio intrusion into the SCS on a longer time scale, when diapycnal mixing processes would become significant.

Supplementary material related to this article is available online at: http://www.biogeosciences-discuss.net/10/6939/2013/bgd-10-6939-2013-supplement.pdf.

Acknowledgements. This study was funded by the National Basic Research Program of China (973 Program) through grant #2009CB421200 and by the National Natural Science Foundation of China through grants # 41130857, 41121091 and 41023007. We are grateful to the captain and crew members on R/V Dongfanghong II as well as H. Lin, X. Huang, Y. Xu, J. Lin and A. Han for their assistance in sampling and/or analyses during the cruises. J. Hu provided the CTD data. We thank K.-K. Liu, T.-D. Qu, C. Measure, P. Cai, Y. Li, H. Lin, H. Gupta and G. Wang for their valuable suggestions. J. Hodgkiss is thanked for his help with the English.

BGD
10, 6939–6972, 2013

References

Baringer, M. O. and Price, J. F.: A review of the physical oceanography of the Mediterranean outflow, Mar. Geol., 155, 63–82, 1999.

Bourgault, D., Hamel, C., Cyr, F., Tremblay, J. É., Galbraith, P. S., Dumont, D., Gratton, Y.: Turbulent nitrate fluxes in the Amundsen Gulf during ice-covered conditions, Geophys. Res. Lett., 38, L15602, doi:10.1029/2011GL047936, 2011.

Cai, W. J., Dai, M. H., Wang, Y. C., Zhai, W. D., Huang, T., Chen, S. T., Zhang, F., Chen, Z. Z., and Wang, Z. H.: The biogeochemistry of inorganic carbon and nutrients in the Pearl River estuary and the adjacent Northern South China Sea, Cont. Shelf Res., 24, 1301–1319, 2004.

Cao, Z. M. and Dai, M. H.: Shallow-depth $CaCO_3$ dissolution: evidence from excess calcium in the South China Sea and its export to the Pacific Ocean, Global Biogeochem. Cy., 25, GB2019, doi:10.1029/2009GB003690, 2011.

Centurioni, L. R., Niiler, P. P., and Lee, D. K.: Observations of inflow of Philippine Sea surface water into the South China Sea through the Luzon Strait, J. Phys. Oceanogr., 34, 113–121, 2004.

Chao, S. Y., Shaw, P. T., and Wu, S. Y.: El Niño modulation of the South China Sea circulation, Prog. Oceanogr., 38, 51–93, doi:10.1016/S0079-6611(96)00010-9, 1996.

Chen, C. T. A. and Huang, M. H.: A mid-depth front separating the South China Sea water and the West Philippine Sea water, J. Oceanogr., 52, 17–25, 1996.

Chen, C. T. A., Wang, S. L., Wang, B. J., and Pai, S. C.: Nutrient budgets for the South China Sea basin, Mar. Chem., 75, 281–300, 2001.

Chen, Y. L.: Spatial and seasonal variations of nitrate-based new production and primary production in the South China Sea, Deep-Sea Res. Pt. I., 52, 319–340, 2005.

Chen, Y. L. and Chen, H. Y.: Seasonal dynamics of primary and new production in the northern South China Sea: the significance of river discharge and nutrient advection, Deep-Sea Res. Pt. I., 53, 971–986, 2006.

Chen, Y. L., Chen, H. Y., Tuo, S., and Ohki, K.: Seasonal dynamics of new production from Trichodesmium N_2 fixation and nitrate uptake in the upstream Kuroshio and South China Sea basin, Limnol. Oceanogr., 53, 1705–1721, 2008.

Chu, P. C. and Li, R. F.: South China Sea isopycnal-surface circulation, J. Phys. Oceanogr., 30, 2419–2438, 2000.

BGD
10, 6939–6972, 2013

Dai, M., Meng, F., Tang, T., Kao, S.-J., Lin, J., Chen, J., Huang, J.-C., Tian, J., Gan, J., and Yang, S.: Excess total organic carbon in the intermediate water of the South China Sea and its export to the North Pacific. Geochem. Geophy. Geosy., 10, Q12002, doi:10.1029/2009GC002752, 2009.

Feely, R. A., Sabine, C. L., Lee, K., Millero, F. J., Lamb, M. F., Greeley, D., Bullister, J. L., Key, R. M., Peng, T. H., Kozyr, A., Ono, T., and Wong, C. S.: In situ calcium carbonate dissolution in the Pacific Ocean, Global Biogeochem. Cy., 16, 1144, doi:10.1029/2002GB001866, 2002.

Glover, D. M., Jenkins, W. J., and Doney, S. C.: Modeling methods for marine science, Cambridge University Press, Cambridge, 255 pp., 2005.

Gong, G. C., Liu, K. K., Liu, C. T., and Pai, S. C.: The chemical hydrography of the South China Sea west of Luzon and a comparison with the West Philippine Sea, Terr. Atmos. Ocean. Sci., 3, 587–602, 1992.

Gordon, A. L.: Circulation of the Caribbean Sea, J. Geophys. Res., 72, 6207–6223, 1967.

Han, A. Q., Dai, M. H., Kao, S. J., Gan, J. P., Li, Q., Wang, L. F., Zhai, W. D., and Wang, L.: Nutrient dynamics and biological consumption in a large continental shelf system under the influence of both a river plume and coastal upwelling, Limnol. Oceanogr., 57, 486–502, doi:10.4319/lo.2012.57.2.0486, 2012.

Hu, J. Y., Kawamura, H., Hong, H. S., and Qi, Y. Q.: A review on the currents in the South China Sea: seasonal circulation, South China Sea warm current and Kuroshio intrusion, J. Oceanogr., 56, 607–624, 2000.

Huertas, I. E., Ríos, A. F., García-Lafuente, J., Navarro, G., Makaoui, A., Sánchez-Román, A., Rodriguez-Galvez, S., Orbi, A., Ruíz, J., and Pérez, F. F.: Atlantic forcing of the Mediterranean oligotrophy, Global Biogeochem. Cy., 26, GB2022, doi:10.1029/2011GB004167, 2012.

Kao, S. J., Yang, J. Y. T., Liu, K. K., Dai, M. H., Chou, W. C., Lin, H. L., and Ren, H.: Isotope constraints on particulate nitrogen source and dynamics in the upper water column of the oligotrophic South China Sea, Global Biogeochem. Cy., 26, GB2033, doi:10.1029/2011GB004091, 2012.

Kara, A. B., Rochford, P. A., and Hurlburt, H. E.: An optimal definition for ocean mixed layer depth, J. Geophys. Res., 105, 16803–16821, doi:10.1029/2000JC900072, 2000.

Kida, S., Yang, J. Y., and Price, J. F.: Marginal sea overflows and the upper ocean interaction, J. Phys. Oceanogr., 39, 387–403, doi:10.1175/2008JPO3934.1, 2009.

BGD
10, 6939–6972, 2013

Lewis, M. R., Harrison, W. G., Oakey, N. S., Hebert, D., and Platt, T.: Vertical nitrate fluxes in the oligotrophic, Science, 234, 870–873, 1986.
Liang, W. D., Yang, Y. J., Tang, T. Y., and Chuang, W. S.: Kuroshio in the Luzon Strait, J. Geophys. Res., 113, C08048, doi:10.1029/2007JC004609, 2008.
Lin, Z. H., Mo, X. G., Li, H. X., and Li, H. B.: Comparison of three spatial interpolation methods for climate variables in China, Acta Geogr. Sin., 57, 47–56, 2002.
Liu, K. K., Chao, S. Y., Shaw, P. T., Gong, G. C., Chen, C. C., and Tang, T. Y.: Monsoon-forced chlorophyll distribution and primary production in the South China Sea: observations and a numerical study, Deep-Sea Res. Pt. I., 49, 1387–1412, 2002.
Liu, Q. Y., Feng, M., and Wang, D. X.: ENSO-induced interannual variability in the southeastern South China Sea, J. Oceanogr., 67, 127–133, doi:10.1007/s10872-011-0002-y, 2011.
Liu, Z. Y. and Lozovatsky, I. D.: Upper pycnocline turbulence in the northern South China Sea, Chinese Sci. Bull., 57, 2302–2306, 2012.
Ma, J., Yuan, D. X., and Liang, Y.: Sequential injection analysis of nanomolar soluble reactive phosphorus in seawater with HLB solid phase extraction, Mar. Chem., 111, 151–159, doi:10.1016/j.marchem.2008.04.011, 2008.
Michael, J. C., Glen, G. G., and Robert, C. B.: Interannual variability of the Kuroshio intrusion in the South China Sea, J. Oceanogr., 62, 559–575, doi:10.1007/s10872-006-0076-0, 2006.
Matsuno, T., Lee, J.-S., and Yanao, S.: The Kuroshio exchange with the South and East China Seas, Ocean Sci., 5, 303–312, doi:10.5194/os-5-303-2009, 2009.
Pratt, L. J. and Spall, M. A.: Circulation and exchange in choked marginal seas, J. Phys. Oceanogr., 38, 2639–2661, doi:10.1175/2008JPO3946.1, 2008.
Qu, T. D.: Upper-layer circulation in the South China Sea, J. Phys. Oceanogr., 30, 1450–1460, 1999.
Qu, T. D., Mitsudera, H., and Yamagata, T.: Intrusion of the North Pacific waters into the South China Sea, J. Geophys. Res., 105, 6415–6424, 2000.
Quigg, A., Finkel, Z. V., Irwin, A. J., Rosenthal, Y., Ho, T. Y., Reinfelder, J. R., Schofield, O., Morel, F. M. M., and Falkowski, P. G.: The evolutionary inheritance of elemental stoichiometry in marine phytoplankton, Nature, 425, 291–294, 2003.
Redfield, A. C., Ketchum, B. H., and Richards, F. A.: The influence of organisms on the composition of seawater, in: The Sea, edited by: Hill, M. N., Wiley, New York, 26–77, 1963.
Schlitzer, R.: Ocean Data View 4, available at: http://odv.awi.de, 2012.

BGD
10, 6939–6972, 2013

Shaw, P. T.: The seasonal variation of the intrusion of the Philippine Sea water into the South China Sea, J. Geophys. Res., 96, 821–827, doi:10.1029/90JC02367, 1991.

Thingstad, T. F., Krom, M. D., Mantoura, R. F. C., Flaten, G. A. F., Groom, S., Herut, B., Kress, N., Law, C. S., Pasternak, A., Pitta, P., Psarra, S., Rassoulzadegan, F., Tanaka, T., Tselepides, A., Wassmann, P., Woodward, E. M. S., Wexels Riser, C., Zodiatis, G., and Zohary, T.: Nature of phosphorus limitation in the ultraoligotrophic eastern mediterranean, Science, 309, 1068–1071, 2005.

Tian, J. W., Yang, Q. X., Liang. X. F., Xie, L. L., Hu, D. X., Wang, F., and Qu, T. D.: Observation of Luzon Strait transport, Geophys. Res. Lett., 33, L19607, doi:10.1029/2006GL026272, 2006.

Tian, J. W., Yang, Q. X., and Zhao, W.: Enhanced diapycnal mixing in the South China Sea, J. Phys. Oceanogr., 39, 3191–3203, doi:10.1175/2009JPO3899.1, 2009.

Tseng, C. M., Wong, G. T. F., Lin, I. I., Wu, C. R., and Liu, K. K.: A unique seasonal pattern in phytoplankton biomass in low-latitude waters in the South China Sea, Geophys. Res. Lett., 32, L08608, doi:10.1029/2004GL022111, 2005.

Wong, G. T. F., Tseng, C. M., Wen, L. S., and Chung, S. W.: Nutrient dynamics and N-anomaly at the SEATS station, Deep-Sea Res. Pt. II., 54, 1528–1545, doi:10.1016/j.dsr2.2007.05.011, 2007.

Wu, J. F., Chung, S. W., Wen, L. S., Liu, K. K., Chen, Y. L., Chen, H. Y., and Karl, D. M.: Dissolved inorganic phosphorus, dissolved iron, and Trichodesmium in the oligotrophic South China Sea, Global Biogeochem. Cy., 17, 1008, doi:10.1029/2002GB001924, 2003.

BGD
10, 6939–6972, 2013

Table 1. Summary of the area-integrated nutrient inventories in the upper 100 m of the water column in the central northern South China Sea.

Seasons	Inventory (10^9 mol)			Reduction relative to summer (%)		
	N + N	SRP	$Si(OH)_4$	N + N	SRP	$Si(OH)_4$
Spring	69	5.8	106	13.2	10.8	10.1
Summer	80	6.5	118	–	–	–
Fall	67	6.2	98	16.2	5.7	17.1
Winter	55	3.6	58	31.7	44.4	51.0

BGD
10, 6939–6972, 2013

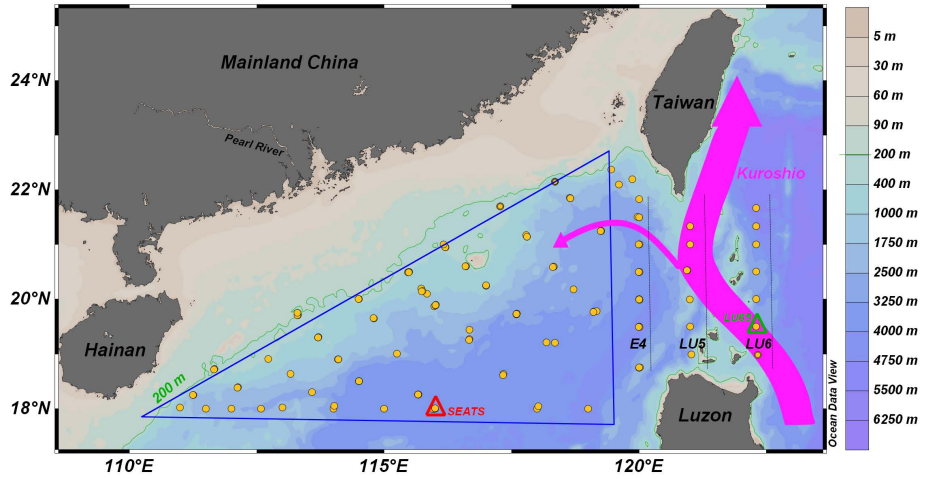

Fig. 1. Map of the northern South China Sea (NSCS) showing its topography and the locations of the sampling stations (yellow dots). The blue triangle indicates the focused region in which the nutrient inventory was assessed. Three meridional sections across the Luzon Strait are highlighted with dark dotted lines (i.e. sections E4, LU5 and LU6, among which sections LU5 and LU6 were investigated only in spring 2011). Also shown schematically are the Kuroshio Current and its intrusion path into the NSCS around the Luzon Strait (pink lines). The South East Asian Time-series Study (SEATS) station (red triangle) is established in the central basin of the SCS, while station LU65 (green triangle) is located in the Kuroshio travel path.

BGD
10, 6939–6972, 2013

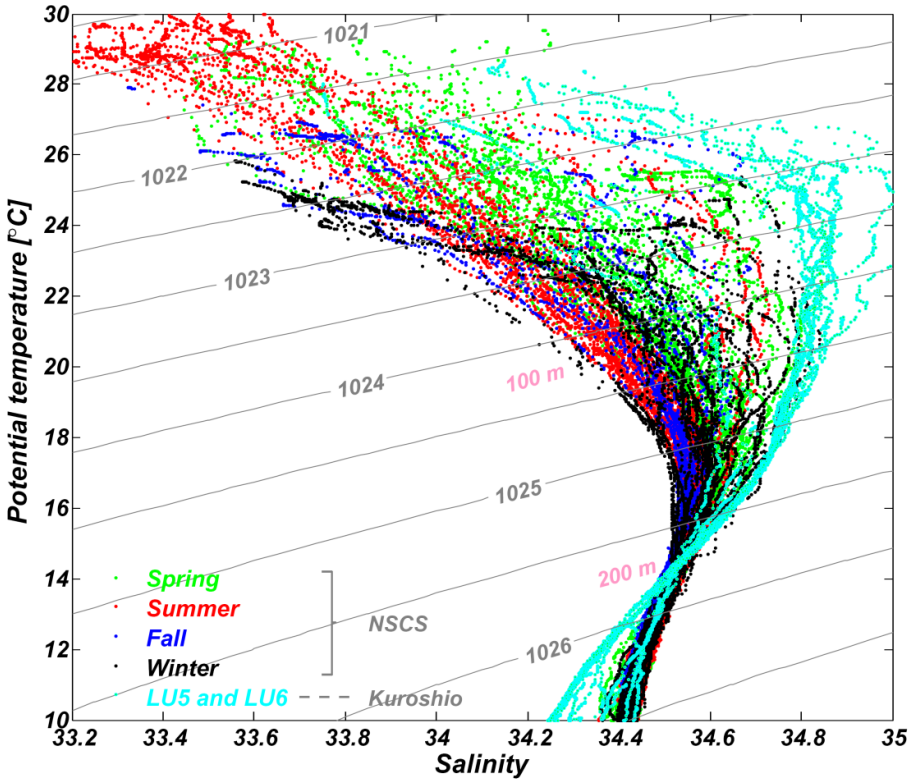

Fig. 2. Potential temperature (θ) versus salinity plots (θ–S diagram) in the upper 400 m of the water column for the sampling stations in the central northern South China Sea (NSCS) during four seasons and along sections LU5 and LU6 in spring. Also marked are the depths of 100 m (density 1024.2 kg m^{-3}) and 200 m (density 1025.6 kg m^{-3}) in the central NSCS.

BGD
10, 6939–6972, 2013

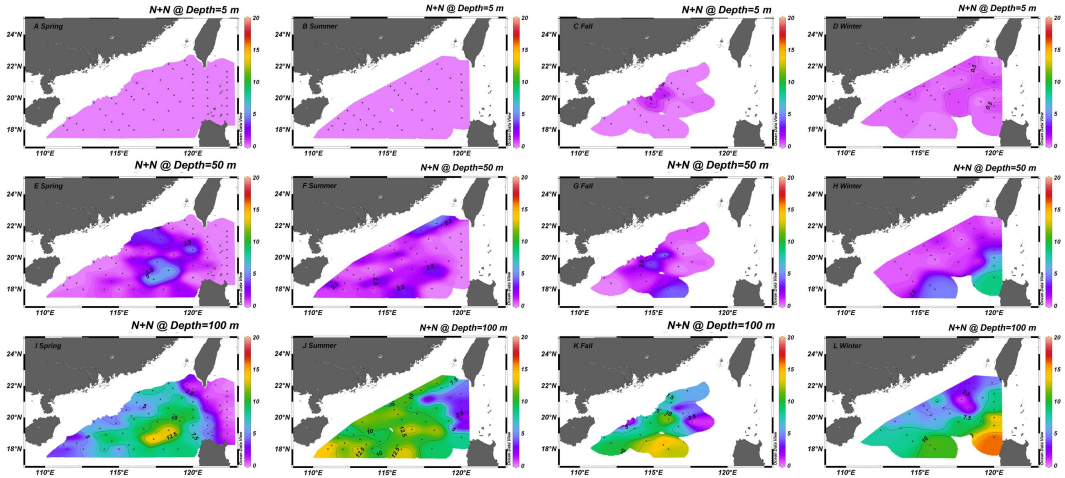

Fig. 3. Iso-depth distributions of N + N (nitrate plus nitrite, μmol L^{-1}) concentrations at depths of 5 m **(A–D)**, 50 m **(E–H)** and 100 m **(I–L)** in the central northern South China Sea and Kuroshio during the four seasons (spring: **A**, **E** and **I**; summer: **B**, **F** and **J**; fall: **C**, **J** and **K**; winter: **D**, **H** and **L**).

BGD
10, 6939–6972, 2013

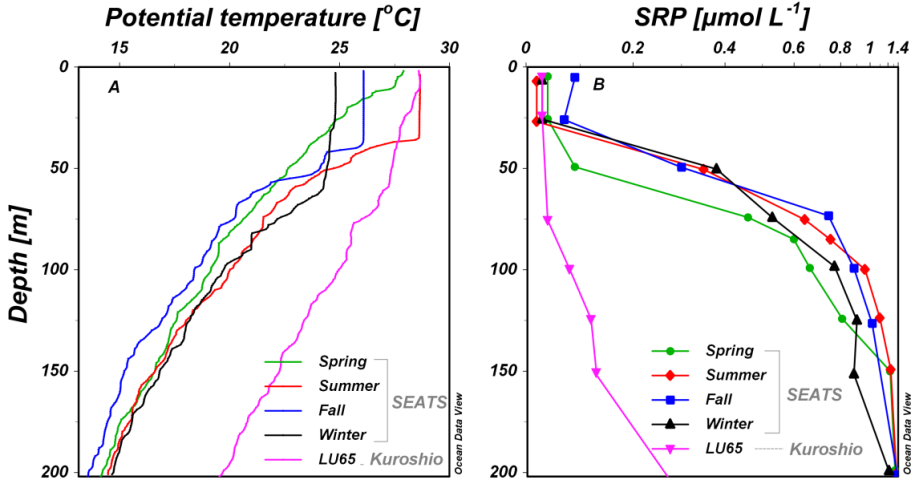

Fig. 4. Vertical distribution of potential temperature **(A)** and SRP (soluble reactive phosphate, **B**) in the upper 200 m of the water column at the SEATS station in different seasons and station LU65 in spring.

BGD
10, 6939–6972, 2013

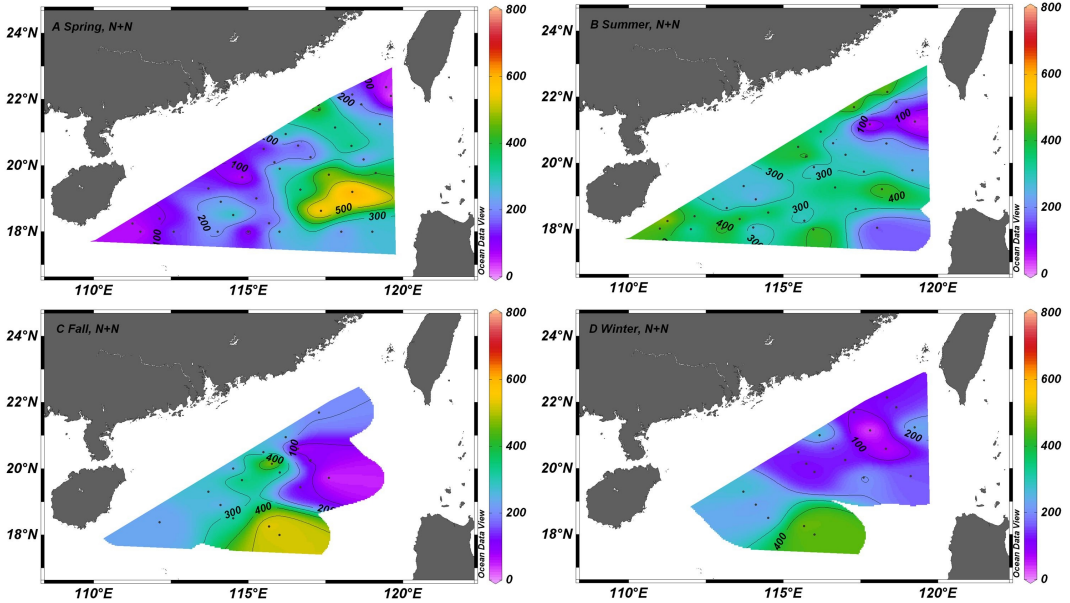

Fig. 5. Station-integrated N + N inventory (mmol m^{-2}) in the upper 100 m of the water column in the central northern South China Sea. **(A)** spring; **(B)** summer; **(C)** fall; and **(D)** winter.

BGD
10, 6939–6972, 2013

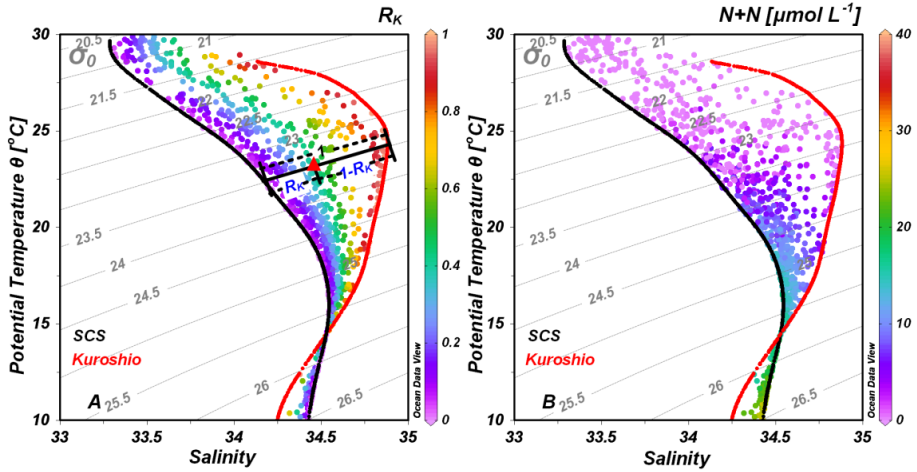

Fig. 6. Potential temperature (θ) versus salinity plots (θ–S diagram) in the upper 400 m of the water column for the sampling stations in the central northern South China Sea (NSCS) superimposed by **(A)** the isopycnal mixing model derived Kuroshio water fraction (R_K), and **(B)** the field observed N + N (nitrate plus nitrite) concentrations. A red triangle in **(A)** donates an example of the R_K calculation along the potential density 1023.5 surface. Data of the typical Kuroshio water were collected from LU6 section in spring, while data of the SCS proper water were collected from station SEATS and its nearby stations in summer.

BGD
10, 6939–6972, 2013

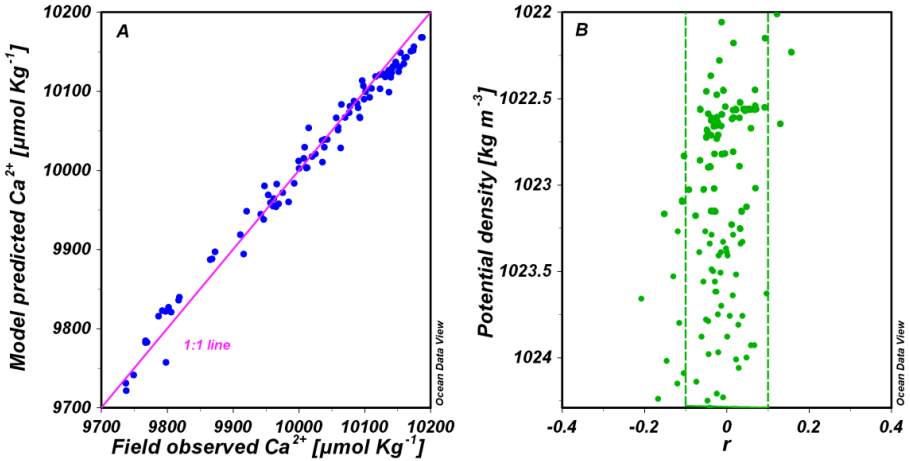

Fig. 7. (A) Scatter plot of the isopycnal mixing predicted Ca^{2+} and the field observed Ca^{2+} in the upper 100 m of the central NSCS. **(B)** The individual error of the estimated Kuroshio water fraction (r) versus potential density in the upper 100 m of the central South China Sea (SCS). Green lines donate the ±0.1 range. Note that the analytical precision of Ca^{2+} is better than ±5 µmol kg^{-1} (Cao and Dai, 2011), which accounts for less than 2 % of the estimated error.

BGD
10, 6939–6972, 2013

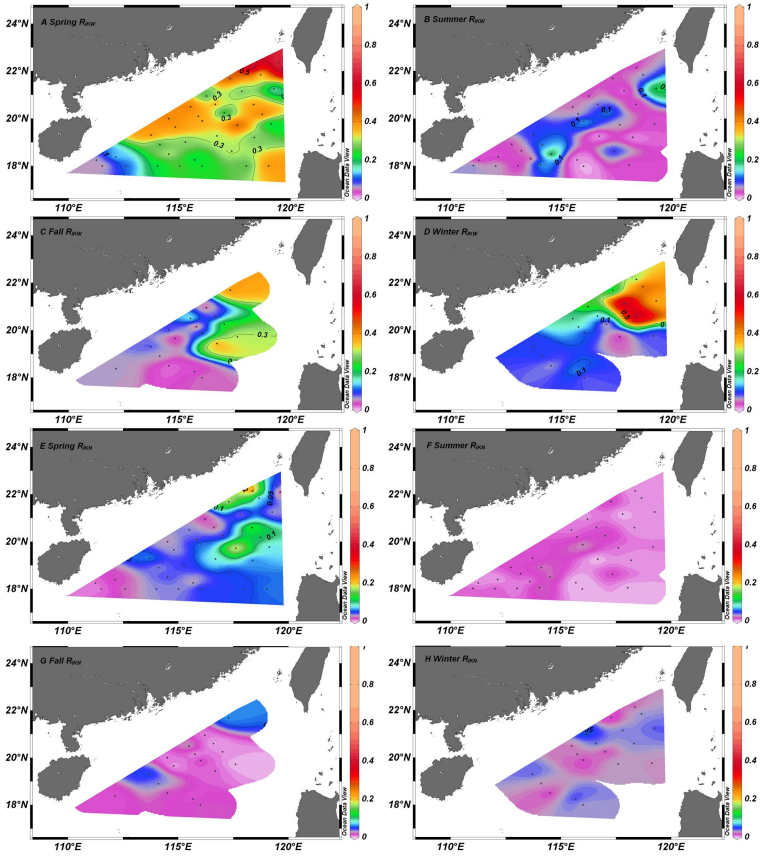

Fig. 8. The station-integrated Kuroshio water fraction (R_{IKW}, **A–D**) and nutrient fraction (R_{IKN}, **E–H**) in the upper 100 m of the central northern South China Sea. **(A)** spring R_{IKW}; **(B)** summer R_{IKW}; **(C)** fall R_{IKW}; **(D)** winter R_{IKW}; **(E)** spring R_{IKN}; **(F)** summer R_{IKN}; **(G)** fall R_{IKN}; and **(H)** winter R_{IKN}.

BGD
10, 6939–6972, 2013

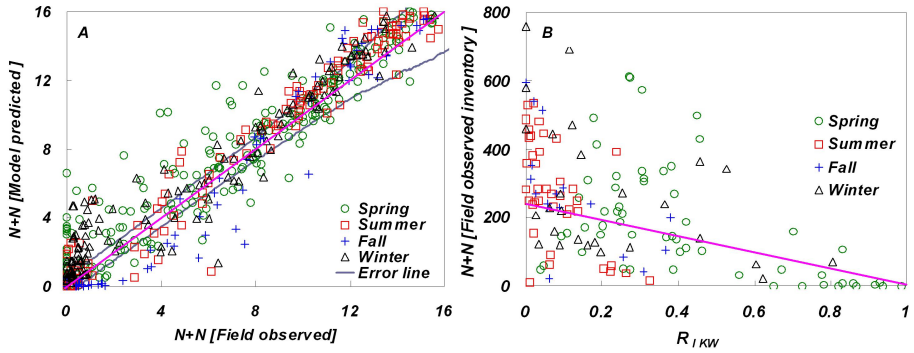

Fig. 9. (A) The model predicted N + N concentrations versus the field measurements in the upper 100 m of the central northern South China Sea (NSCS). Pink line is the 1 : 1 line while gray lines donate the $X_r \pm S_r$ domain; **(B)** the relationship between the field observed N + N inventory and the station-integrated Kuroshio water fraction (R_{IKW}). Pink line is the theoretical mixing line constructed by the N + N inventory of the SCS and Kuroshio end-members ($\sim 250\,\mathrm{mmol\,m^{-2}}$ in NSCS and $\sim 5\,\mathrm{mmol\,m^{-2}}$ in Kuroshio, respectively, which is obtained by supposing the mixing R_{KW} is the same value in the entire upper 100 m).

BGD
10, 6939–6972, 2013

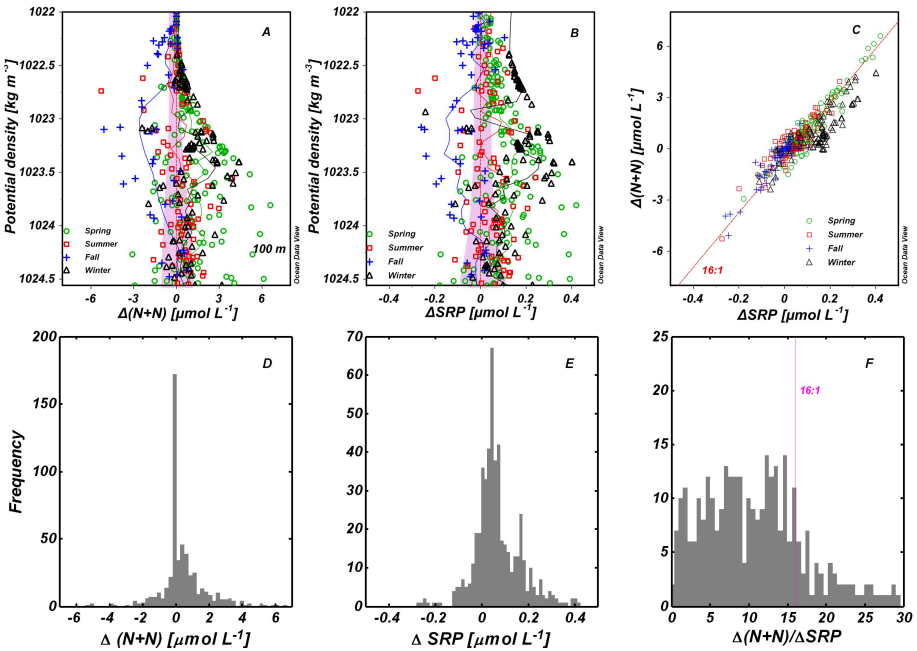

Fig. 10. Δ(N + N) **(A)** and ΔSRP **(B)** versus potential density in the upper 100 m of the central NSCS. **(C)** The relationship between Δ(N + N) and ΔSRP. Lines in A and B represent the moving average during each season. Pink shadows in **(A)** and **(B)** indicate the $X_N \pm S_N$ domain (see Supplement for details). The straight pink line in **(C)** denotes the theoretical correlation of 16 : 1 based on the Redfield ratio (Redfield et al., 1963). Also shown are the histogram distributions of Δ(N + N) **(D)**, ΔSRP **(E)** and Δ(N + N)/ΔSRP **(F)** in the upper 100 m of the central NSCS.

BGD
10, 6939–6972, 2013